XVI International Conference on Computational Plasticity. Fundamentals and Applications
COMPLAS 2021
E. Oñate, D. Peric, M. Chiumenti and Eduardo de Souza Neto (Eds)

HOMOGENIZATION BASED TWO-SCALE MODELLING OF FLUID-SATURATED POROUS MEDIA WITH SELF-CONTACT AND FLOW IN MICROPORES

EDUARD ROHAN* **AND JAN HECZKO***

*Department of Mechanics & NTIS New Technologies for Information Society, Faculty of Applied Sciences, University of West Bohemia in Pilsen,
Univerzitní 8, 30100 Plzeň, Czech Republic
rohan@kme.zcu.cz

Key words: Unilateral contact; Porous media, Multiscale modeling, Homogenization, Fluid-structure interaction; Semi-smooth Newton method

Abstract. The contribution is devoted to the homogenization and the two-scale numerical modelling of fluid-saturated porous media subject to static loads which, at the pore level, induce unilateral self-contact. The initial microstructure is periodic, being generated by a representative cell consisting of elastic skeleton and a rigid inclusion which is anchored in the skeleton on a part of its pore surface. The unilateral frictionless contact interaction is considered between the inclusion and the elastic skeleton on matching surfaces. Depending on the deformation due to applied macroscopic loads, the self-contact interaction alters the one between the solid and fluid phases. Both the disconnected and connected porosities are treated. The two-scale limit model is presented in detail for structures of the first type which do not allow for the fluid mass redistribution. Numerical examples of 2D deforming structures are presented.

1 INTRODUCTION

Porous materials with the self-contact interaction in the microstructure present a challenging issue for the homogenization-based two scale modelling. The literature devoted to this topic is not vast. Fissured media were treated in [10] using the formal approach of asymptotic expansion, leading to the homogenized macroscopic variational inequality. Further contributions to the frictionless self-contact problem with soft, or hard inclusions were handled using the two-scale convergence in [7], or matched asymptotic expansions [1]. In [3], the theoretical homogenization result was extended using the periodic unfolding method [2] for problems with friction and possibly rotating rigid inclusions, cf. [6]. The computational homogenization approach to solving the contact problems was considered in [11], and [5].

In our recent study [8], we proposed a two-scale model of dry porous elastic medium with local self-contacts at the pores scale of the periodic structure. Therein, an incremental algorithm was proposed which involves a consistent tangent modulus of the elastic medium with a "frozen sliding contact" constraining the macroscopic step of the two scale computational procedure.

As a new contribution, here we consider a fluid-saturated porous elastic material subject to external loads inducing the self-contact interaction at the pore level. Its microstructure is constituted as a periodic lattice generated by a representative cell consisting of a solid skeleton and a fluid-filled pore. On its surface, the unilateral frictionless contact appears when the porous material is deformed. We focus on microstructures with rigid inclusions whereby the contact process involves opposing surfaces on the rigid and the compliant skeleton parts. A macroscopic model is derived using the periodic unfolding homogenization and the method of oscillating test functions which has been applied in [8]. Both the disconnected and connected porosities are treated; in the latter case, quasistatic fluid flow is described by the Stokes model. A homogenized model is derived using the periodic unfolding and the method of oscillating test functions. The macroscopic model attains the form of a nonlinear Biot continuum, whereby the Darcy flow model governs the fluid redistribution. However, this study focuses on the microstructures with disconnected porosities saturated by a slightly compressible fluid.

We propose an efficient algorithm for two-scale computational analysis with the numerical model obtained using the FE discretization of the homogenized model. For this, a sequential linearization is used which leads to consistent stiffness matrices of the macroscopic elasticity problem. At the local level, the contact problem attains the form of a nonsmooth equation which is solved using the semi-smooth Newton method [4] without any regularization, or a problem relaxation.

Basic notations By $x = (x_1, \dots, x_d) \in \mathbb{R}^d$ we denote spatial coordinates at the macroscale, while $y = (y_1, \dots, y_d)$ specifies the zoomed "microscopic" coordinates in the sense of the unfolding method of homogenization [2]. We use $\nabla = \nabla_x = (\partial_i^x)$ and $\nabla_y = (\partial_i^y)$ to denote gradients with respect to these coordinates.

2 SELF-CONTACT IN POROUS MEDIUM

An open bounded domain $\Omega \subset \mathbb{R}^d$, with the dimension $d = 2, 3$, is constituted by the solid skeleton Ω_s and by the fluid occupying domain Ω_f, so that

$$\Omega = \Omega_s^\varepsilon \cup \Omega_f^\varepsilon \cup \Gamma^\varepsilon \,, \quad \Omega_s^\varepsilon \cap \Omega_f^\varepsilon = \emptyset \,, \quad \overline{\Omega_f^\varepsilon} \subset \Omega \,, \tag{2.1}$$

where $\Gamma^\varepsilon = \partial\Omega_s^\varepsilon \cap \partial\Omega_f^\varepsilon$ is the interface. The solid part Ω_s^ε is generated as a periodic lattice by repeating the representative volume element (RVE) occupying domain $Z^\varepsilon = \varepsilon Y$. The zoomed cell $Y = \Pi_{i=1}^3]0, \bar{y}_i[\subset \mathbb{R}^3$ splits into the solid part occupying domain Y_s and the complementary fluid part Y_f, see Fig. 1, thus

$$Y = Y_s \cup Y_f \cup \Gamma^Y \,, \quad Y_s = Y \setminus Y_f \,, \quad \Gamma_Y = \overline{Y_s} \cap \overline{Y_f} \,. \tag{2.2}$$

We assume that Ω_s^ε is a connected domain, whereas domain Ω_f^ε can be connected (a channel network, thus $\partial Y_f \cap \partial Y \neq \emptyset$), or it can be constituted as a periodic array of disconnected fluid inclusions, thus $\overline{Y_f} \subset Y$.

To impose boundary conditions on the external surface of Ω, the decomposition of the boundary is introduced, $\partial\Omega = \partial_u\Omega \cup \partial_\sigma\Omega$, $\partial_u\Omega \cap \partial_\sigma\Omega = \emptyset$. The fluid-structure interface

Γ^ε splits in two parts: the self-contact can be attained on Γ^ε_c, whereas Γ^ε_f, is a part of Γ^ε on which any contact is excluded,

$$\Gamma^\varepsilon_f = \Gamma^\varepsilon \setminus \Gamma^\varepsilon_c \,, \quad \Gamma^\varepsilon_+ = \Gamma^\varepsilon_c \setminus \Gamma^\varepsilon_- \,, \quad \Gamma^\varepsilon_+ \cap \Gamma^\varepsilon_- = \emptyset \,. \tag{2.3}$$

Γ^ε_c splits into two disjoint parts, such that, in the deformed configuration, points on Γ^ε_+ can get in contact with those situated on Γ^ε_-. The contact gap is introduced using the jump $[\boldsymbol{u}]^\varepsilon_n = \boldsymbol{n}(x^-)\cdot(\boldsymbol{u}(x^+) - \boldsymbol{u}(x^-))$, $x^+ \in \Gamma^\varepsilon_+$, $x^- \in \Gamma^\varepsilon_-$, where $\boldsymbol{n}$ is the unit normal.

2.1 Micromodel for disconnected pores – static problem

We assume that the pores Ω^ε_f are filled with slightly compressible fluid, compressibility modulus γ is given. In the solid phase loaded by body forces $\boldsymbol{f}^\varepsilon$ and external surface traction forces $\boldsymbol{b}$, the displacement field $\boldsymbol{u}^\varepsilon$ satisfies the following relationships,

$$\begin{aligned} \nabla\cdot\boldsymbol{\sigma}^\varepsilon + \boldsymbol{f}^\varepsilon = \boldsymbol{0} \quad & \text{in } \Omega^\varepsilon_s \,, \\ \boldsymbol{u}^\varepsilon = \boldsymbol{0} \quad & \text{on } \partial_u\Omega_s \,, \\ \boldsymbol{\sigma}^\varepsilon\cdot\boldsymbol{n} = \boldsymbol{b}^\varepsilon \quad & \text{on } \partial_\sigma\Omega_s \,, \end{aligned} \tag{2.4}$$

and the fluid-structure interaction including the unilateral self-contact conditions,

$$\begin{aligned} \boldsymbol{\sigma}^\varepsilon\cdot\boldsymbol{n} = -p^\varepsilon \quad & \text{on } \Gamma^\varepsilon_f \,, \\ g^\varepsilon_c(\boldsymbol{u}^\varepsilon)\le 0 \,, \quad \sigma^\varepsilon_n \le -p^\varepsilon \,, \quad g^\varepsilon_c(\boldsymbol{u}^\varepsilon)(\sigma^\varepsilon_n + p^\varepsilon) = 0 \quad & \text{on } \Gamma^\varepsilon_c \,, \\ \boldsymbol{\sigma}^\varepsilon : \boldsymbol{n}\otimes\boldsymbol{t} = 0 \quad & \text{on } \Gamma^\varepsilon_c \,, \end{aligned} \tag{2.5}$$

where $g^\varepsilon_c(\boldsymbol{v})(x) = [\boldsymbol{v}(x)]^\varepsilon_n - [x]^\varepsilon_n$ is the gap function defined on Γ^ε_c. By $\boldsymbol{\sigma}^\varepsilon = \mathbb{D}^\varepsilon\boldsymbol{e}(\boldsymbol{u}^\varepsilon)$ we denote the stress tensor involving the strain $\boldsymbol{e}(\boldsymbol{u}^\varepsilon)$. The contact stress $\sigma^\varepsilon_n = \boldsymbol{n}\otimes\boldsymbol{n} : \boldsymbol{\sigma}^\varepsilon$ is the stress projection in the normal direction determined by $\boldsymbol{n} = \boldsymbol{n}^{[\mathrm{s}]}$, and the tangent $\boldsymbol{t}$ is any unit vector satisfying $\boldsymbol{n}\cdot\boldsymbol{t} = 0$.

The set of displacements satisfying $(2.4)_2$, is denoted by $\mathcal{U}_0(\Omega^\varepsilon_s) = \{\boldsymbol{v}\in\mathbf{H}^1(\Omega^\varepsilon_s)|\ \boldsymbol{u}^\varepsilon = 0 \quad \text{on } \partial_u\Omega^\varepsilon_s\}$. If a part of Ω^ε_s is rigid, the "rigid body motion" constraint applies in $\Omega^{r,\varepsilon}_R$, $r = 1, 2, \ldots$, whereby r refers to a r-th copy of the rigid inclusion $Z^\varepsilon_R \subset Z^\varepsilon_s$. By $\mathcal{R}^\varepsilon(\Omega^\varepsilon_s)$ we denote a space of rigid body displacement fields defined in each $\Omega^{r,\varepsilon}_R$.

To establish in the whole domain Ω a pressure field defined in the voids, we define $\Omega^{k,\varepsilon}$ as a k-th copy of the reference cell Z^ε placed at position x^k in the periodic lattice; By $\Omega^{k,\varepsilon}_f \subset \Omega^{k,\varepsilon}$ we refer to the k-th fluid inclusion. Pressure p^ε is related to the displacement field due to the mass conservation,

$$\int_{\partial\Omega^{k,\varepsilon}_f} \boldsymbol{u}^\varepsilon\cdot\boldsymbol{n}^{[\mathrm{s}]} = \gamma p^\varepsilon|\Omega^{k,\varepsilon}_f| \,, \quad \forall k = 1, 2, \ldots, \bar{k}^\varepsilon \,, \tag{2.6}$$

where γ is the fluid compressibility. We assume that for $\boldsymbol{u}^\varepsilon \equiv 0$ (unloaded structure) the pressure vanishes in all pores, *i.e.* $p^\varepsilon = 0$.

The homogenization procedure is applied to the weak formulation of problem (2.4)-(2.6) which is now introduced. For this, the set $\mathcal{K}^\varepsilon$ comprising kinematically admissible displacements and the space $\mathcal{Q}^\varepsilon$ of pore pressures is needed,

$$\begin{aligned}\mathcal{K}^\varepsilon &= \{\boldsymbol{v} \in \mathcal{U}_0(\Omega_s^\varepsilon) \cap \mathcal{R}(\Omega_s^\varepsilon) |\ \boldsymbol{v} = 0 \text{ on } \partial_u\Omega_s^\varepsilon\ ,\ g_c^\varepsilon(\boldsymbol{v}) \le 0 \ \text{ on } \Gamma_c^\varepsilon\}\ ,\\ \mathcal{Q}^\varepsilon &= \{q \in L^2(\Omega) |\ q \text{ is constant in each } \Omega^{k,\varepsilon}\ ,\ k = 1, 2, \dots, \bar{k}^\varepsilon\}\ ,\end{aligned} \tag{2.7}$$

The displacement field $\boldsymbol{u}^\varepsilon \in \mathcal{K}^\varepsilon$ and the pressure $p^\varepsilon \in \mathcal{Q}^\varepsilon$ is called a weak solution to Problem (2.4)-(2.6) when it satisfies the variational inequality,

$$\begin{aligned}a_\Omega^\varepsilon(\boldsymbol{u}^\varepsilon, \boldsymbol{v}^\varepsilon - \boldsymbol{u}^\varepsilon) + \int_{\partial\Omega_f^\varepsilon} p^\varepsilon \boldsymbol{n}^{[\mathrm{s}]} \cdot (\boldsymbol{v}^\varepsilon - \boldsymbol{u}^\varepsilon) \ge \int_{\Omega_s^\varepsilon} \boldsymbol{f}^\varepsilon \cdot (\boldsymbol{v}^\varepsilon - \boldsymbol{u}^\varepsilon) + \int_{\partial_\sigma\Omega} \boldsymbol{b} \cdot (\boldsymbol{v}^\varepsilon - \boldsymbol{u}^\varepsilon)\ , \quad \forall \boldsymbol{v}^\varepsilon \in \mathcal{K}^\varepsilon\ ,\\ \int_{\partial\Omega_f^\varepsilon} q^\varepsilon \boldsymbol{u}^\varepsilon \cdot \boldsymbol{n}^{[\mathrm{s}]} - \gamma \int_{\Omega_f^\varepsilon} p^\varepsilon q^\varepsilon = 0 \quad \forall q^\varepsilon \in \mathcal{Q}^\varepsilon\ ,\\ \text{where} \quad a_\Omega^\varepsilon(\boldsymbol{w}, \boldsymbol{v}) = \int_{\Omega_s^\varepsilon \setminus \Omega_R^\varepsilon} \mathbb{D}\boldsymbol{e}(\boldsymbol{w}) : \boldsymbol{e}(\boldsymbol{v})\ .\end{aligned} \tag{2.8}$$

2.2 Micromodel for steady flow in connected pores

The flow in collapsible channels, here presented by the contact gap, belongs to singularly perturbed problems which are cumbersome to solve. Instead of defining a free boundary problem, we consider a relaxed problem imposed in the deformed configuration, namely in the deformed pores $\tilde{\Omega}_f^\varepsilon$. Let $\Omega_C^\varepsilon \subset \Omega_f^\varepsilon$ be a subdomain occupied by the fluid "between" the two matching surfaces Γ_+^ε and Γ_-^ε of the contact area, so that $\Omega_f^\varepsilon = \Omega_C^\varepsilon \cup \Omega_F^\varepsilon \cup \Gamma_{FC}^\varepsilon$, where Ω_F^ε denotes the uncollapsible part of the porosity. We establish a nondegenerate domain $\tilde{\Omega}_{C,\delta}^\varepsilon$ in the deformed configuration. For this, we consider $\psi_\delta^\varepsilon \in C_0^\infty(\Gamma_-^\varepsilon)$, such that $\psi_\delta^\varepsilon = 0$ on $\partial\Gamma_-^\varepsilon$, while $\psi_\delta^\varepsilon = \delta$ in $\Gamma_{-,\delta}^\varepsilon \subset \partial\Gamma_-^\varepsilon$, where $\mathrm{dist}(\partial\Gamma_{-,\delta}^\varepsilon, \partial\Gamma_-^\varepsilon) = \delta$. We define $\tilde{\Omega}_{C,\delta}^\varepsilon(\boldsymbol{v}) = \{x \in \mathbb{R}^3, x = \xi - \boldsymbol{n}^-(\xi)(g_c^\varepsilon(\boldsymbol{v}) - \psi_\delta^\varepsilon(\xi)), \xi \in \Gamma_-^\varepsilon\}$. Parameter $\delta > 0$ presents the minimum gap clearance; we consider $\delta = \varkappa\varepsilon$ with a given proportion $0 < \varkappa << 1$, therefore we can drop δ from the notation. Now the relaxed deformed fluid domain $\tilde{\Omega}_f^\varepsilon(\boldsymbol{v}) = \tilde{\Omega}_C^\varepsilon \cup \tilde{\Omega}_F^\varepsilon \cup \tilde{\Gamma}_{FC}^\varepsilon$ associated with a displacement field can be obtained using a smooth mapping $\varphi^\varepsilon(\boldsymbol{v}) : \Omega_f^\varepsilon \mapsto \tilde{\Omega}_f^\varepsilon$, in particular $\tilde{\Omega}_f^\varepsilon \ni z = \varphi^\varepsilon(\boldsymbol{v}, x)$ for $x \in \Omega_f^\varepsilon$, assuming a sufficiently smooth field $\boldsymbol{v}$ defined in Ω_f^ε.

The viscous fluid flow in the fluid channels (pores) requires a slight modification of condition (2.4)-(2.5) to respect the fluid stress $\boldsymbol{\tau}^\varepsilon = -p^\varepsilon \boldsymbol{I} + \mu^\varepsilon \boldsymbol{e}(\boldsymbol{v}^{f,\varepsilon})$ depending on the fluid velocity $\boldsymbol{v}^{f,\varepsilon}$ and viscosity $\mu^\varepsilon = \varepsilon^2\bar{\mu}$, so that

$$\begin{aligned}(\boldsymbol{\sigma}^\varepsilon - \boldsymbol{\tau}^\varepsilon) \cdot \boldsymbol{n} = 0 \quad \text{on } \Gamma_f^\varepsilon\ , \quad \boldsymbol{t} \cdot (\boldsymbol{\sigma}^\varepsilon - \boldsymbol{\tau}^\varepsilon) \cdot \boldsymbol{n} = 0 \quad \text{on } \Gamma_c^\varepsilon\ ,\\ g_c^\varepsilon(\boldsymbol{u}^\varepsilon) \le 0\ , \quad \sigma_n^\varepsilon \le \tau_n^\varepsilon\ , \quad g_c^\varepsilon(\boldsymbol{u}^\varepsilon)(\sigma_n^\varepsilon - \tau_n^\varepsilon) = 0 \quad \text{on } \Gamma_c^\varepsilon\ ,\end{aligned} \tag{2.9}$$

where $\tau_n^\varepsilon = \boldsymbol{n} \otimes \boldsymbol{n} : \boldsymbol{\tau}^\varepsilon = -p^\varepsilon + \mu^\varepsilon \boldsymbol{e}(\boldsymbol{v}^{f,\varepsilon}) : \boldsymbol{n} \otimes \boldsymbol{n}$. Instead of (2.6), the Stokes flow of an incompressible viscous fluid in the deformed channels is considered,

$$\mu^\varepsilon \nabla^2 \boldsymbol{v}^{f,\varepsilon} - \nabla p^\varepsilon + \boldsymbol{f}^\varepsilon = \boldsymbol{0}\ , \quad \nabla \cdot \boldsymbol{v}^{f,\varepsilon} = 0 \quad \text{in } \tilde{\Omega}_f^\varepsilon(\boldsymbol{u}^\varepsilon)\ , \quad \boldsymbol{v}^{f,\varepsilon} = \boldsymbol{0} \quad \text{on } \tilde{\Gamma}^\varepsilon(\boldsymbol{u}^\varepsilon)\ , \tag{2.10}$$

where the no slip condition holds in the steady state, since $\dot{\boldsymbol{u}}^\varepsilon = \mathbf{0}$. Due to the assumed smooth mapping $\varphi^\varepsilon(\boldsymbol{u}^\varepsilon)$, the associated transformation of coordinates enables to rewrite (2.10) in the undeformed configuration Ω_f^ε. In any case, the homogenization of the fluid and the solid responses is tightly coupled.

3 HOMOGENIZATION

Homogenization of the considered two-phase medium with the self-contact and the fluid-structure interactions is treated in analogy with the void-pore situation reported in [8]. Here we focus on the case of non-connected pores, problem (2.4)-(2.6). We only present resulting model equations and formulate problems to be solved numerically by a tow-scale computational procedure, see Section 4.

The limit problem is defined in terms of global macroscopic coordinates $x \in \Omega$, and the local microscopic ones $y \in Y$. Formally, the local (microscopic) and global (macroscopic) problems can be derived using asymptotic expansions combined with the periodic unfolding technique; using the unfolding operator $\mathcal{T}_\varepsilon()$, we consider

$$\mathcal{T}_\varepsilon(\boldsymbol{u}^\varepsilon(x)) = \boldsymbol{u}^0(x) + \varepsilon \boldsymbol{u}^1(x,y) + \varepsilon^2(\dots \ ,$$

where $\boldsymbol{u}^0 \in \mathbf{H}^1(\Omega)$ and $\boldsymbol{u}^1 \in L^2(\Omega; \mathbf{H}^1_\#(Y_s))$. The same form of the expansion (3) is used to define the test functions $\boldsymbol{v}^\varepsilon$. For any $D \subset Y$, $\mathbf{H}^1_\#(D)$ designates the Sobolev space $\boldsymbol{W}^{1,2}(Y) = \mathbf{H}^1(Y)$ of vector-valued Y-periodic functions (indicated by the subscript #) defined in D. Integral $\fint_D = |Y|^{-1}\int_D$ gives the mean value.

For the case of nonempty rigid inclusions $Y_R \subset Y_s$, let $Y_S = Y_s \setminus Y_R$ and $\mathcal{R}_\#(Y_s, Y_R) = \mathbf{H}^1_\#(Y_s) \cap \mathcal{R}(Y_R)$ be the restriction of $\mathbf{H}^1_\#(Y_s)$ to displacements $\boldsymbol{u}^1(x,\cdot)$ constraint by a rigid body motion in Y_R. Let $\phi_{RF} = (|Y_f| + |Y_R|)/|Y| = \phi_F + \phi_R$, hence $\phi_S = 1 - \phi_{RF}$ is the volume fraction of the compliant solid.

3.1 Local contact problems

We can introduce the gap function and the associated convex set $\mathcal{K}_Y$,

$$\begin{aligned} \mathcal{K}_Y(\nabla \boldsymbol{u}) &= \{\boldsymbol{v} \in \mathcal{R}_\#(Y_s, Y_R) | g_c^Y(\boldsymbol{v}, \nabla \boldsymbol{u}) \le 0\} \ , \\ \text{where} \quad g_c^Y(\boldsymbol{u}^1, \nabla \boldsymbol{u}^0) &= \left[\nabla \boldsymbol{u}^0 \widehat{y} + \boldsymbol{u}^1 - \widehat{y}\right]_n^Y \ , \end{aligned} \tag{3.1}$$

where $[\boldsymbol{w}]_n^Y = \boldsymbol{n} \cdot (\boldsymbol{w}|_+ - \boldsymbol{w}|_-)$ is the contact gap jump on Γ_c. The asymptotic homogenization based on the unfolding technique leads to the local contact problem for microstructures with rigid inclusions. For a.a. $x \in \Omega$, the fluctuating displacement fields $\boldsymbol{u}^1(x,\cdot) \in \mathcal{K}_Y(\nabla \boldsymbol{u}^0)$, satisfy

$$a^F_{Y_S}\left(\boldsymbol{u}^1 + \boldsymbol{\Pi}^{ij} e^x_{ij}(\boldsymbol{u}^0),\ \boldsymbol{v} - \boldsymbol{u}^1\right) - \frac{1}{\gamma \phi_f} \delta_{ij} e^x_{ij}(\boldsymbol{u}^0) \fint_{Y_S} \nabla_y \cdot (\boldsymbol{v} - \boldsymbol{u}^1) \ge 0 \ , \tag{3.2}$$

for all $\boldsymbol{v} \in \mathcal{K}_Y(\nabla \boldsymbol{u}^0)$, where $\boldsymbol{\Pi}^{ij} = (\Pi^{ij}_k)$, $i,j,k = 1,2,3$ with its components $\Pi^{ij}_k = y_j \delta_{ik}$, and

$$\begin{aligned} a^F_{Y_S}(\boldsymbol{u},\, \boldsymbol{v}) &= a_{Y_S}(\boldsymbol{u},\, \boldsymbol{v}) + \frac{1}{\gamma\phi_f} \fint_{Y_S} \nabla_y \cdot \boldsymbol{u} \fint_{Y_S} \nabla_y \cdot \boldsymbol{v} \,, \\ a_{Y_S}(\boldsymbol{u},\, \boldsymbol{v}) &= \fint_{Y_S} (\mathbb{D}\boldsymbol{e}_y(\boldsymbol{u})) : \boldsymbol{e}_y(\boldsymbol{v}) \,. \end{aligned} \tag{3.3}$$

3.2 Macroscopic problem and incremental subproblems

The global (macroscopic) model equation involving $\boldsymbol{u}^0$ and $\boldsymbol{u}^1$ is derived from (2.8) by choosing a special interplay between the test functions $\boldsymbol{v}^0$ and $\boldsymbol{v}^1$ which are coupled by virtue of the gap function. The two fields $\boldsymbol{u}^0 \in U(\Omega)$ and $\boldsymbol{u}^1 \in L^2(\Omega; \mathcal{K}_Y(\nabla \boldsymbol{u}^0))$ satisfy

$$\begin{aligned} \int_\Omega \boldsymbol{\sigma}^0(\boldsymbol{u}^0, \boldsymbol{u}^1) : \boldsymbol{e}_x(\boldsymbol{v}^0) - \frac{1}{\gamma\phi_f} \int_\Omega \left(\fint_{Y_S} \nabla_y \cdot \boldsymbol{u}^1 - \phi_{RF} \nabla_x \cdot \boldsymbol{u}^0 \right) \phi_{RF} \nabla_x \cdot \boldsymbol{v}^0 \\ = \int_\Omega \bar{\boldsymbol{f}} \cdot \boldsymbol{v}^0 + \int_{\partial_\sigma \Omega} \boldsymbol{b} \cdot \boldsymbol{v}^0 \quad \forall \boldsymbol{v} \in U_0(\Omega) \,. \end{aligned} \tag{3.4}$$

where $\boldsymbol{\sigma}^0(\boldsymbol{u}^0, \boldsymbol{u}^1) = |Y|^{-1} \int_{Y_S} \mathbb{D}(\boldsymbol{e}_y(\boldsymbol{u}^1) + \boldsymbol{e}_x(\boldsymbol{u}^0))$ is the mean stress and the pressure $p^0(x)$ of the pore fluid can be determined for a.a. $x \in \Omega$,

$$\phi_{RF} \nabla_x \cdot \boldsymbol{u}^0 - \fint_{Y_S} \nabla_y \cdot \boldsymbol{u}^1 + \gamma\phi_f p^0 = 0 \,. \tag{3.5}$$

Small perturbations $\delta\boldsymbol{u}^0$ and $\delta\boldsymbol{u}^1 = \boldsymbol{w}^{ij} e^x_{ij}(\delta\boldsymbol{u}^0)$ are related by a "linearized" contact problem which yields the corrector problem for $\boldsymbol{w}^{ij}$ introduced below, see (3.10). Let $r(\boldsymbol{v}^0)$ be the out-of-balance functional,

$$r(\boldsymbol{v}^0) := \int_\Omega \boldsymbol{f} \cdot \boldsymbol{v}^0 + \int_{\partial_\sigma \Omega} \boldsymbol{b} \cdot \boldsymbol{v}^0 - \int_\Omega \widetilde{\boldsymbol{\sigma}}^{\rm tot} : \boldsymbol{e}_x(\boldsymbol{v}^0) \,, \tag{3.6}$$

where the total stress $\boldsymbol{\sigma}^{\rm tot} = \boldsymbol{\sigma}^0 - p^0 \phi_{RF} \boldsymbol{I}$ evaluated for the current approximation of the two-scale solution $(\widetilde{\boldsymbol{u}}^0, \widetilde{\boldsymbol{u}}^1)$ is denoted by $\widetilde{\boldsymbol{\sigma}}^{\rm tot}$; note that $\widetilde{p}^0$ is determined for $\widetilde{\boldsymbol{u}}^0$ by virtue of (3.5). Thus, $\boldsymbol{\sigma}^{\rm tot} := \widetilde{\boldsymbol{\sigma}}^{\rm tot}(\widetilde{\boldsymbol{u}}^0) + \delta\boldsymbol{\sigma}^{\rm tot}$ with $\delta\boldsymbol{\sigma}^{\rm tot} := \mathbb{D}^H \boldsymbol{e}_x(\delta\boldsymbol{u}^0)$ involving the tangential stiffness effective modulus $\mathbb{D}^H = (D^H_{ijkl})$ defined below. The perturbation $\delta\boldsymbol{u}^0 \in U_0(\Omega)$ satisfies the macroscopic incremental problem,

$$\int_\Omega \mathbb{D}^H \boldsymbol{e}_x(\delta\boldsymbol{u}^0) : \boldsymbol{e}_x(\boldsymbol{v}^0) = r(\boldsymbol{v}^0) \,, \quad \forall \boldsymbol{v} \in U_0(\Omega) \,. \tag{3.7}$$

3.3 Effective tangent stiffness

To compute the tangent stiffness, the following problem must be solved: Find $\boldsymbol{w}^{ij}(x, \cdot) \in V_0(\boldsymbol{\Pi}^{ij}, Y_S, x)$, $i,j = 1, \ldots, d$ which satisfy

$$\fint_{Y_S} \mathbb{D}\boldsymbol{e}_y(\boldsymbol{w}^{ij} + \boldsymbol{\Pi}^{ij}) : \boldsymbol{e}_y(\boldsymbol{v}) + \frac{1}{\gamma\phi_f} \left(\fint_{Y_S} \nabla_y \cdot \boldsymbol{w}^{ij} - \phi_{RF}\delta_{ij} \right) \fint_{Y_S} \nabla_y \cdot \boldsymbol{v} = 0 \,, \tag{3.8}$$

for all $\boldsymbol{v} \in V_0(0, Y_S, x)$, where the set of admissible displacement perturbations is introduced for the actual contact surface $\Gamma_c^*(x) \subset \Gamma_c$,

$$V_0(\boldsymbol{U}, Y_s, x) = \{\boldsymbol{v} \in \mathbf{H}^1_{\#}(Y_s) |\ [\boldsymbol{v} + \boldsymbol{U}]_n^{(Y)} = 0 \text{ on } \Gamma_c^*(x)\} \ . \tag{3.9}$$

In analogy with the local contact problem expressed using the bilinear form (3.3), problem (3.8) can be rewritten, as follows: Find $\boldsymbol{w}^{ij}(x, \cdot) \in V_0(\boldsymbol{\Pi}^{ij}, Y_S, x)$, $i, j = 1, \ldots, d$ which satisfy

$$a^F_{Y_S}\left(\boldsymbol{w}^{ij} + \boldsymbol{\Pi}^{ij},\ \boldsymbol{v}\right) - \frac{1}{\gamma\phi_f}\delta_{ij} \fint_{Y_S} \nabla_y \cdot \boldsymbol{v} = 0 \ , \tag{3.10}$$

for all $\boldsymbol{v} \in V_0(0, Y_S, x)$. Now, using correctors $\boldsymbol{w}^{ij}$, the tangential stiffness effective modulus, $\mathbb{D}^H = (D^H_{ijkl})$ is computed

$$\begin{aligned} D^H_{ijkl} = {} & a_{Y_S}\left(\boldsymbol{w}^{ij} + \boldsymbol{\Pi}^{ij},\ \boldsymbol{w}^{kl} + \boldsymbol{\Pi}^{kl}\right) \\ & + \frac{1}{\gamma\phi_f}\left(\fint_{Y_S} \nabla_y \cdot \boldsymbol{w}^{ij} - \phi_{RF}\delta_{ij}\right)\left(\fint_{Y_S} \nabla_y \cdot \boldsymbol{w}^{kl} - \phi_{RF}\delta_{kl}\right) \ . \end{aligned} \tag{3.11}$$

3.4 Two-scale incremental computational algorithm

By virtue of the small deformation assumption, we use the initial configuration associated with the "unfolded" domain $\Omega \times Y$ as the reference one. The local contact problems (3.2), with actual contact gaps depending on the macroscopic deformation, are solved in micro-configurations $\widetilde{\mathcal{M}}_Y(x)$ at Selected Macroscopic Points (SMP) $x \in \Omega$ associated with the numerical discretization. This step is commuted by solving the global problem (3.7) in Ω. The following Algorithm has been implemented.

1. Initialization: set data; put $\tilde{\boldsymbol{u}}^0 = 0$ in Ω and $\tilde{\boldsymbol{u}}^1 = 0$.

2. Given local micro-configurations $\widetilde{\mathcal{M}}_Y(x)$ and an approximation $\tilde{\boldsymbol{u}}^0$ at SMP $x \in \Omega$, compute $\boldsymbol{u}^1(x, \cdot)$ solve local contact problems (3.2), with the initial guess $\tilde{\boldsymbol{u}}^1$ (to initiate the semi-smooth Newton method).

3. For SMP $x \in \Omega$, update the micro-configurations: $\widetilde{Y}_s(x) = Y_s + \{\tilde{\boldsymbol{u}}^{\rm mic}(x, \cdot)\}_{Y_s}$ with $\tilde{\boldsymbol{u}}^{\rm mic}(x, \cdot) := \boldsymbol{\Pi}^{ij} e^x_{ij}(\boldsymbol{u}^0) + \boldsymbol{u}^1$. This yields the actual true contact boundary $\Gamma_c^*(x)$. Compute the tangent stiffness $\mathbb{D}^H(x)$ by solving linear problems (3.10) and using (3.11). Update the total effective stress $\tilde{\boldsymbol{\sigma}}^0(x)$.

4. Compute the correction $\delta\boldsymbol{u}^0 \in U_0(\Omega)$ by solving (3.7) which depends on the out-of-balance $\tilde{r}(\boldsymbol{v})$, see (3.6).

5. Update $\boldsymbol{u}^0 = \tilde{\boldsymbol{u}}^0 + \delta\boldsymbol{u}^0$, hence $\tilde{\boldsymbol{u}}^0 := \boldsymbol{u}^0$. Check the convergence ($\delta\boldsymbol{u}^0$ being small); if NOT converged, GO TO Step 2.

3.5 Homogenization of the steady flow in collapsible pores

Homogenization of the fluid-structure interaction, as described by (2.4), (2.9) and (2.10), presents a cumbersome problem introducing an additional nonlinearity since the flow in the contact gap is described in the deformed configuration $\tilde{\Omega}_f^\varepsilon$. Nevertheless, a sequential linearization enables to derive formally a two scale model which leads to a computational procedure similar to the one announced above. Below we make a reference to corresponding Steps of the Algorithm presented in Section 3.4.

Besides the displacements $\boldsymbol{u}^0(x)$ and $\boldsymbol{u}^1(x,y)$, pressure $p^0(x)$ and the seepage flow velocity $\boldsymbol{w}(x,y)$ are involved in the local problems to be solved at SMP $x \in \Omega$. Since the fluid-structure interaction phenomenon is the same as in the non-contact situation, cf. [9], assuming a given reference configuration, *i.e.* an approximation of $\tilde{\Omega}_f^\varepsilon$, hence also $\tilde{Y}_f(x)$ for the fluid subproblem, similar arguments justify a separate treatment of the flow and the solid-contact problems, thus, being interconnected by the macroscopic pressure $p^0(x)$ only. In analogy to (3.2), see Step 2 of the Algorithm, local problems have to be solved for given $(\tilde{\boldsymbol{u}}^0, \tilde{p}^0)$. The fluctuations $\boldsymbol{u}^1(x,\cdot) \in \mathcal{K}_Y(\nabla\tilde{\boldsymbol{u}}^0)$ satisfy the variational inequality

$$a_{Y_S}\left(\boldsymbol{u}^1 + \boldsymbol{\Pi}^{ij} e^x_{ij}(\tilde{\boldsymbol{u}}^0),\, \boldsymbol{v} - \boldsymbol{u}^1\right) + \tilde{p}^0 \fint_{Y_S} \nabla_y \cdot (\boldsymbol{v} - \boldsymbol{u}^1) \geq 0\,, \quad \forall \boldsymbol{v} \in \mathcal{K}_Y(\nabla\tilde{\boldsymbol{u}}^0)\,. \tag{3.12}$$

The macroscopic incremental problem analogous to (3.7), see Step 4, attains the form a modified Biot-Darcy model. It involves the static permeability computed for the reference deformed microstructure, and the (drained) elasticity $\mathbb{D}^H$ and the Biot stress coefficients $\mathbb{B}^H$ which are obtained by homogenizing the porous structure, as in the linear case, however, using the kinematic constraint due to the set (3.9). Within one increment, the Darcy flow problem is solved, which yields an updated $p^0(x)$. Then $\delta\boldsymbol{u}^0 \in U_0(\Omega)$ is solved,

$$\int_\Omega \mathbb{D}^H \boldsymbol{e}_x(\delta\boldsymbol{u}^0) : \boldsymbol{e}_x(\boldsymbol{v}^0) = r(\boldsymbol{v}^0) + \int_\Omega p^0 \mathbb{B}^H : \boldsymbol{e}_x(\boldsymbol{v}^0)\,, \quad \forall \boldsymbol{v} \in U_0(\Omega)\,, \tag{3.13}$$

where $r(\boldsymbol{v}^0)$ is given as in (3.6). Consequently, the deformed configuration $\tilde{Y}_f$ is updated, in analogy with Step 3.

4 NUMERICAL EXAMPLES

For illustration of the two-scale model reported in Section 3, we present simulations of 2D structures with disconnected inclusions. Under obvious symmetry assumptions and consistently with the presence of rigid inclusions, the 2D problems describe 3D structures under the plane strain conditions. The material properties are given by the Young's modulus, $E = 2.3\,\mathrm{GPa}$, the Poisson's ratio, $\nu = 0.35$, and the bulk modulus of the fluid, $K = \gamma^{-1} = 2.2\,\mathrm{GPa}$.

4.1 Periodic cell and micro-problems

The deformable part of the representative cell $Y =]0,1[\times]0,1[$ is partitioned by a triangular finite element mesh, which is shown in Fig. 1. The contact region Γ_{cS}, the deformable-rigid interface Γ_{R}, and the parts of domain boundary, on which boundary conditions are applied, are highlighted.

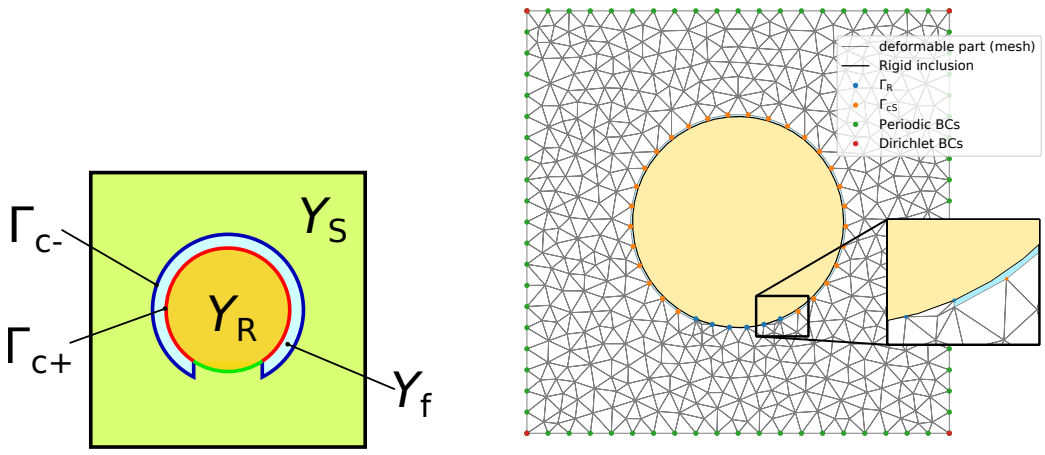

Figure 1: Periodic unit cell Y ad its decomposition (left), see (2.2). The actual finite element mesh (right). Note the thin gap Y_f between the matching contact surfaces, Γ_{c+} and Γ_{c-} .

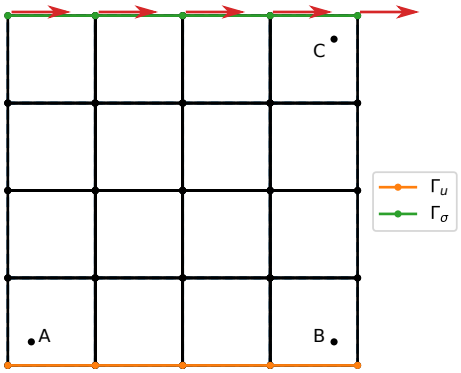

Figure 2: Macroscopic finite element mesh and positions A,B, and C, see Fig. 4.

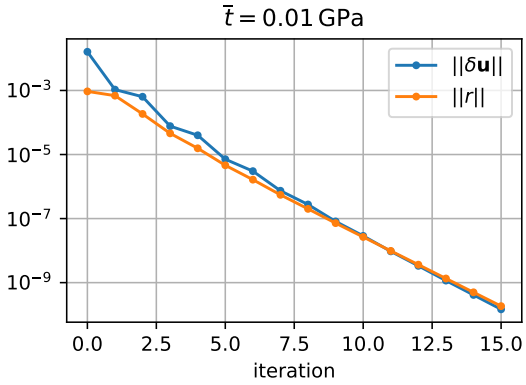

Figure 3: Convergence criteria in the case of fluid-filled structure.

4.2 Macroscopic response

We consider a short cantilever beam subject to a bending. In the 2D setting, the porous structure occupies domain $\Omega =]0, L[\times]0, L[$, $L = 1\text{m}$. Displacements are fixed on its bottom edge, $\boldsymbol{u} = \boldsymbol{0}$ on $\Gamma_u = \{x \in \partial\Omega | x_2 = 0\}$. On its top edge $\Gamma_\sigma = \{x \in \partial\Omega | x_2 = L\}$, the structure is loaded by uniform tractions tangential to the surface $\overline{\mathbf{b}} = \big(\bar{t}, 0\big)$. The numerical model is obtained by the finite element discretization [8]. Being approximated using the linear triangular elements, the local micro-problems are imposed at all Gauss points of the the macroscopic finite element mesh, see Fig. 2, corresponding to the Q1 conforming approximation, thus, four micro-problems to be solved per one macro-element. Hence, the simulations required 64 local contact problems to be solved in any macroscopic iteration. To display local responses, selected locations – points A, B, and C, are indicated for further reference in Fig. 2, where also the surfaces Γ_u and Γ_σ are highlighted.

The total loading by traction $\bar{t} = 10^{-2}\,\text{GPa}$ was split into five steps; in each one, the

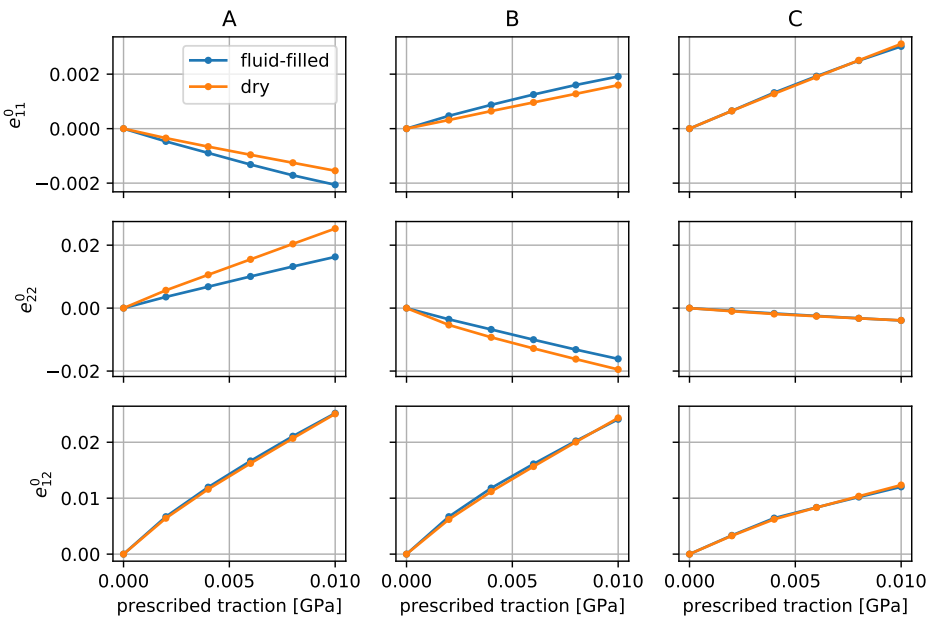

Figure 4: Histories of macroscopic strain components at the three selected points (see Fig. 2). Two simulations are compared: with dry and with fluid-filled pores.

Algorithm presented in Section 3.4 was performed. The convergence of the two-scale iterations are shown in Fig. 3 for the case of fluid-filled pores. Within 15 iterations, the out-of balance r, as well as the macroscopic corrections $\delta\boldsymbol{u}^0$ converged with global tolerances $\|\delta\boldsymbol{u}^0\| < \epsilon_u = 10^{-8}$ m and $\|r\| < \epsilon_r = 10^{-10}$ GPa.

Fig. 4 shows the histories of macroscopic strain components at the selected locations, A, B, and C, for both the dry and the fluid-filled pores cases; note that the dry case, as described in [8], is comprised formally in the fluid-filled inclusion model with the infinite compressibility, thus, when putting $\gamma = \infty$. The effect of the presence of the fluid is mostly seen at the base of the structure (points A and B).

The fluid in pores also modifies the redistribution of the contact stress in the microstructure when compared with the dry-pore situation. Fig. 5 shows the numbers of the mesh nodes in contact in the simulations with dry or fluid-filled pores, microscopic solutions, and fluid pressure distribution in the deformed fluid-saturated porous structure. Stress component σ_{22} and contact pressure are shown in the plots of microscopic solutions. It can be seen that the distribution of tensile stress σ_{22} is more uniform in the microstructure with fluid-filled pores thanks to the load-bearing capacity of the fluid.

5 CONCLUSION

The two-scale model of the homogenized porous medium with self-contact in fluid filed pores has been derived for the linear kinematics of the strain and a linear material behaviour. For the connected porosity which admits the fluid flow, a hybrid treatment with the flow described in the deformed configuration using a relaxed contact gap was

proposed. Numerical solutions of 2D problems are obtained using an iterative algorithm which proved a satisfactory convergence rates, however further improvements are required to enhance its efficiency and robustness.

Acknowledgement The research has been supported by the grant projects GACR 19-04956S and GACR 21-16406S of the Czech Science Foundation.

REFERENCES

[1] Ivan I. Argatov and Taras A. Mel'nyk. Homogenization of a contact problem for a system of densely situated punches. *European Journal of Mechanics - A/Solids*, 20(1):91 – 98, 2001.

[2] D. Cioranescu, A. Damlamian, and G. Griso. The periodic unfolding method in homogenization. *SIAM Journal on Mathematical Analysis*, 40(4):1585–1620, 2008.

[3] D. Cioranescu, A. Damlamian, and J. Orlik. Homogenization via unfolding in periodic elasticity with contact on closed and open cracks. *Asymptotic Analysis*, 82(3-4):201–232, 2013.

[4] T. De Luca, F. Facchinei, and C. Kanzow. A semismooth equation approach to the solution of nonlinear complementarity problems. *Mathematical Programming*, 75(3):407–439, 1996.

[5] G.A. Drosopoulos, P. Wriggers, and G.E. Stavroulakis. A multi-scale computational method including contact for the analysis of damage in composite materials. *Computational Materials Science*, 95:522 – 535, 2014.

[6] G. Griso, A. Migunova, and J. Orlik. Homogenization via unfolding in periodic layer with contact. *Asymptotic Analysis*, 99(1-2):23–52, 2016.

[7] A. Mikelić, M. Shillor, and R. Tapiéro. Homogenization of an elastic material with inclusions in frictionless contact. *Mathematical and Computer Modelling*, 28(4):287 – 307, 1998. Recent Advances in Contact Mechanics.

[8] E. Rohan and J. Heczko. Homogenization and numerical modelling of poroelastic materials with self-contact in the microstructure. *Computers & Structures*, 230:106086, 2020.

[9] E. Rohan and S. Naili. Homogenization of the fluid-structure interaction in acoustics of porous media perfused by viscous fluid. *Zeitschrift für angewandte Mathematik und Physik (ZAMP)*, 71(4):137–164, 2020.

[10] E. Sanchez-Palencia. *Non-homogeneous media and vibration theory*. Number 127 in Lecture Notes in Physics. Springer, Berlin, 1980.

[11] A. Temizer and P. Wriggers. A multiscale contact homogenization technique for the modeling of third bodies in the contact interface. *Computer Methods in Applied Mechanics and Engineering*, 198(3):377 – 396, 2008.

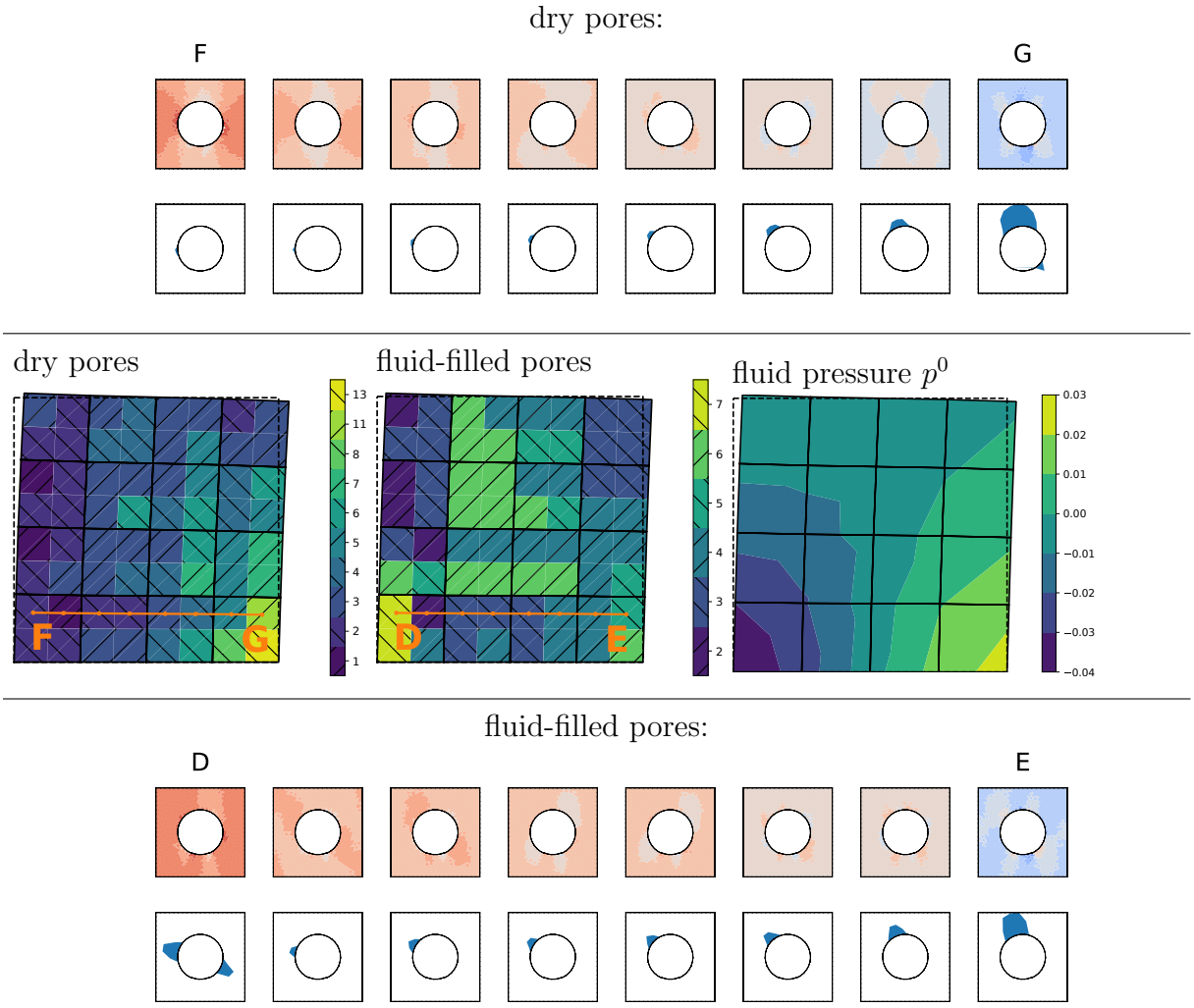

Figure 5: Number of nodes in contact as indicated for the simulations with dry pores (middle row, to the left) and with fluid-filled pores (middle row, center) and the corresponding fluid pressure (middle row, to the right). The top and bottom rows show micro solutions along the D-E (fluid-filled pores) and F-G line (dry pores); stress component σ_{22} and contact tractions are displayed.